Direct Comparison of Au_3^+ and C_{60}^+ Cluster Projectiles in SIMS Molecular Depth Profiling

Juan Cheng and Joseph Kozole
Department of Chemistry, Pennsylvania State University, University Park, Pennsylvania, USA

Robert Hengstebeck
Materials Research Institute, University Park, Pennsylvania, USA

Nicholas Winograd
Department of Chemistry, Pennsylvania State University, University Park, Pennsylvania, USA

The sputtering properties of two representative cluster ion beams in secondary ion mass spectrometry (SIMS), C_{60}^+ and Au_3^+, have been directly compared. Organic thin films consisting of trehalose and dipalmitoylphosphatidylcholine (DPPC) are employed as prototypical targets. The strategy is to make direct comparison of the response of a molecular solid to each type of the bombarding cluster by overlapping the two ion beams onto the same area of the sample surface. The ion beams alternately erode the sample while keeping the same projectile for spectral acquisition. The results from these experiments are important to further optimize the use of cluster projectiles for SIMS molecular depth profiling experiments. For example, Au_3^+ bombardment is found to induce more chemical damage as well as Au implantation when compared with C_{60}^+. Moreover, C_{60}^+ is found to be able to remove the damage and the implanted Au effectively. Discussions are also presented on strategies of enhancing sensitivity for imaging applications with cluster SIMS. (J Am Soc Mass Spectrom 2007, 18, 406–412) © 2007 American Society for Mass Spectrometry

Energetic cluster ion bombardment and secondary ion mass spectrometry (SIMS) experiments have opened new applications in molecular depth profiling and 3D chemical imaging [1–3]. With this approach, it has been reported for many systems, that cluster projectiles remove large amounts of material from molecular solids without the damage accumulation associated with atomic projectiles [4–12]. Moreover, erosion of the material occurs without significant interlayer mixing and/or the formation of topographical features, allowing depth resolution of 10 to 30 nm to be achieved [8–10]. These attributes have compelled a majority of SIMS workers to quickly adopt this new technology.

Although many different cluster projectiles have been examined, practical considerations have led to wide adaptation of liquid metal ion sources consisting of Au or Bi projectiles (Au_3^+ and Bi_3^+, respectively) [13–16], and gas ion sources consisting of SF_5^+ or C_{60}^+ projectiles [6, 17, 18]. The physics of the ion/solid interaction is likely to be quite different between the carbon and metal-type sources since at 20 keV incident energy, each carbon atom carries 333 eV of kinetic energy while each metal atom in a trimer carries 6667 eV of kinetic energy. Moreover, there is a large mass variation between the atoms comprising these cluster species.

The imaging capability of the two types of sources is quite different. The liquid metal ion gun (LMIG) technology yields very bright ion beams with a probe size of less than 100 nm in diameter [19]. The gas ion source requires apertures to define the beam size, sacrificing beam current. Recently, a C_{60} source has been introduced [20] that achieves a submicron probe size with enough current to acquire images in a reasonable amount of time. In general, however, higher lateral resolution is achieved with the LMIG design if there is enough sensitivity in the mass spectrum associated with the smallest resolvable pixel.

It is now well established that many cluster ion sources are capable of molecular depth profiling [9–11]. During removal of material from the sample, chemical damage accumulation normally associated with atomic bombardment is largely avoided, and molecular ion signals persist even after extended periods of ion bombardment. Projectiles with larger numbers of atoms such as C_{60}^+ and Bi_7^+ often leave less accumulated damage than clusters with less numbers of atoms, such as Au_3^+ and Bi_3^+ [5, 9, 15]. It has been proposed that when combining molecular depth profiling with imaging etching should be performed with the C_{60} source, and

Published online November 21, 2006

Address reprint requests to Dr. Juan Cheng, Department of Chemistry, Pennsylvania State University, 104 Chemistry Building, University Park, PA, 16802, USA. E-mail: chengjuan@psu.edu

1044-0305/07/$32.00
doi:10.1016/j.jasms.2006.10.017

Received July 25, 2006
Revised October 16, 2006
Accepted October 19, 2006

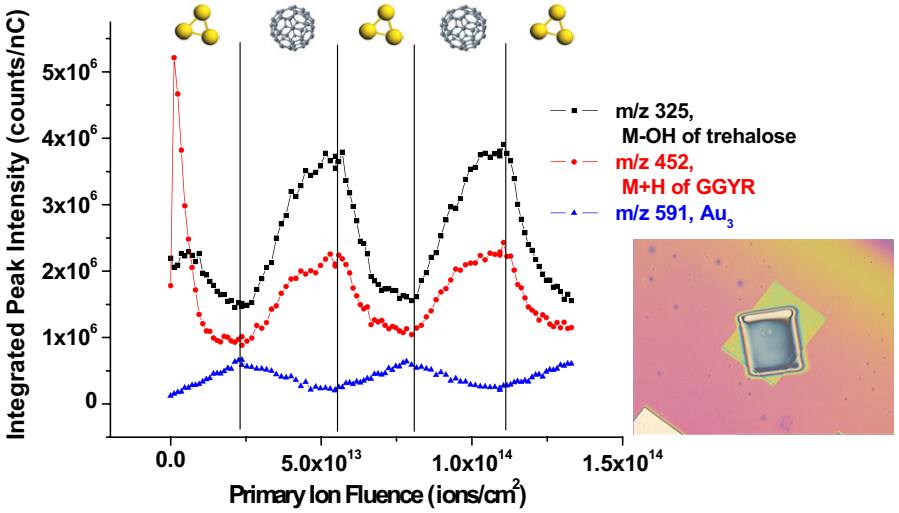

Figure 1. Secondary ion signal intensities are plotted against the primary ion dose during the alternative bombardment by Au_3^+ and C_{60}^+. The order of the projectile that is used to sputter for each turn is indicated on the figure. The inset is an optical image of the film after the overlap depth profile experiment. The smaller crater is created by C_{60}^+ sputtering while the bigger crater on the outside is created by Au_3^+ sputtering. All of the spectra are taken from the overlapped center area. The field of view is 1360 μm $\times$ 1020 μm.

images should be acquired with the LMIG source due to its higher lateral resolution [1, 13, 15].

To establish the fundamental properties associated with these projectiles and to help decide which cluster source is most appropriate for a specific experiment, a comprehensive comparison of the response of a molecular solid to each type of bombarding cluster is needed. Here we provide an approach for direct and efficient comparison of different properties, using C_{60}^+ and Au_3^+ as an example. This strategy is to overlap two ion beams with comparable kinetic energies onto the same area of the sample surface. The method follows the beam overlap procedure previously developed for directly comparing an atomic ion source and a cluster ion source [6, 21, 22]. Direct comparison between ion beams can then be performed by alternating the incident projectile used for erosion while keeping the same analysis projectile for spectral acquisition.

Two model organic thin film systems have been investigated. In the first instance, a 300 nm-peptide-doped trehalose thin film is utilized to assess the relative damage accumulation and efficiency of producing molecular ions with C_{60}^+ or Au_3^+. The trehalose platform has been shown to be particularly well-suited for model studies due to the film uniformity, high sputtering yield and reproducibility [9]. Moreover, it is possible to dope the film with small peptides so as to examine the possibility of depth profiling using relatively fragile biological molecules. In a second instance, a thin film of neat dipalmitoyl-phosphatidylcholine (DPPC) has been examined in a similar fashion. This system is of interest since the film is less-well characterized but represents an important class of biomolecules of interest in 3D imaging experiments [20, 23]. The results show that in all cases the C_{60}^+ projectile yields larger molecular ion signals than Au_3^+ during depth profiling. The result is correlated with attenuated production of fragment ions and the enhanced production of H_3O^+ ions [24]. Measured ion fractions are still quite low even with the cluster sources, about 10^{-5} for all systems, suggesting that image resolution will be limited by sensitivity rather than the physical size of the interrogating probe.

Experimental

Trehalose Film Preparation

A detailed procedure of the preparation of the trehalose films has been described previously [9]. Trehalose and the peptide Gly-Gly-Tyr-Arg (GGYR) were obtained from Sigma-Aldrich (St. Louis, MO). To prepare a trehalose film, peptides were dissolved in water at concentrations of 10 mM and then mixed with the same volume of 1M aqueous trehalose solution. The mixture was then spin-cast onto a presliced 5 mm $\times$ 5 mm Si wafer (Ted Pella Inc., Redding, CA) spinning at a speed of about 3200 rpm. A uniformly colored film with a glassy appearance is normally obtained.

DPPC Film Preparation

A detailed description of the preparation method for dehydrated organic films of the fatty-acid dipalmitoyl-phosphatidylcholine (DPPC) can be found elsewhere [23]. Briefly, the DPPC (Avanti Polar Lipids Inc., Alabaster, AL) films were prepared by spin-casting (3000 rpm spin rate) a lipid chloroform solution (5 mg/mL) onto chemically etched, presliced 5 mm $\times$ 5 mm silicon wafers (Ted Pella Inc.). The resulting dry, porous or-

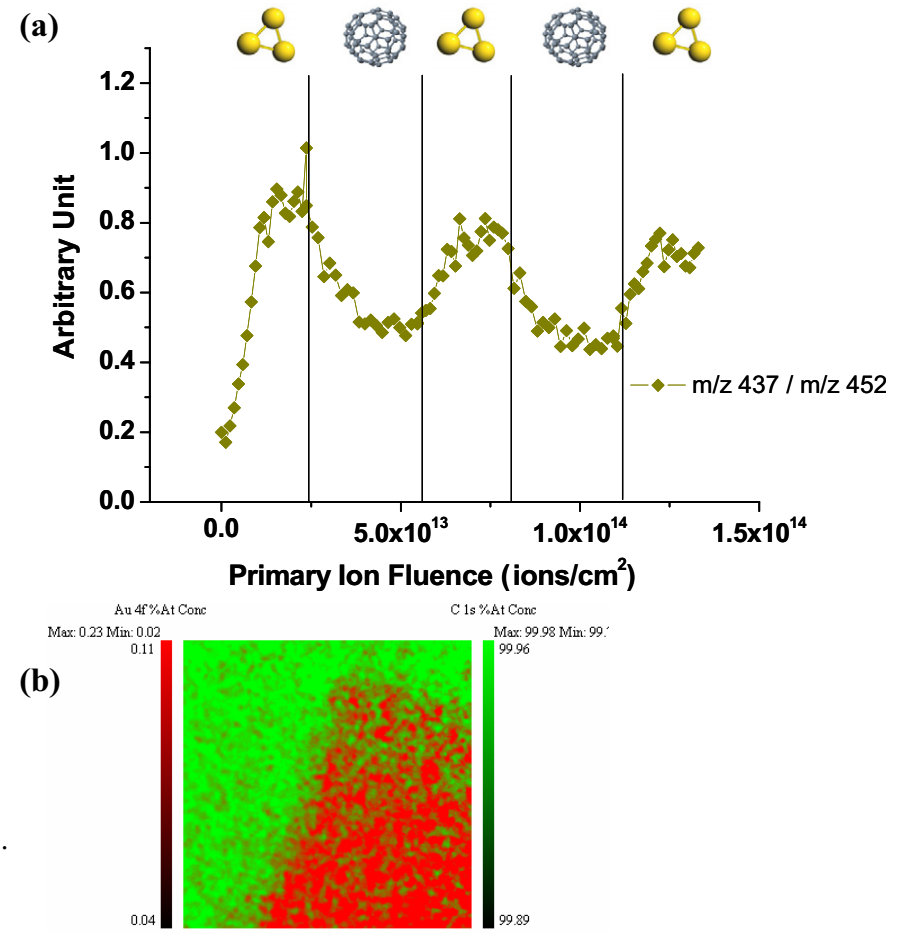

Figure 2. (**a**) Plot of the ratio between *m/z* 437 to *m/z* 452 (M + H of GGYR) versus accumulated total ion dose. (**b**) XPS image of Au (Au 4f in red) and C (C1s in green) from part of the crater after extensive bombardment of Au_3^+. The field of view is 800 μm × 800 μm.

ganic film was measured to be 1000 nm in thickness and to have a 20 to 100 nm surface roughness using atomic force microscopy (Nanopics 2100, TLA Tencor Inc., San Jose, CA).

Instrumentation and Depth-Profiling Experiments

Depth profiles and TOF-SIMS spectra were recorded using previously described instrumentation [8, 25]. Spectra were recorded using 50 ns pulses for bombardment, followed by delayed extraction of secondary ions with a delay of 100 ns. This procedure yields a mass resolution of about 1000 above *m/z* 200. For depth profiling, the two ion sources C_{60}^+ and Au_3^+ are first overlapped to the same spot on the sample surface in the instrument. The sputter area for both ion sources is set to be 600 μm by 600 μm, and the spectra are taken from an area of 100 μm by 100 μm centered within the sputter area using a total fluence of less than 10^{10} ions/cm^2. The software allows dc bombardment with either Au_3^+ or C_{60}^+ while C_{60}^+ is used to collect spectra in all cases. The overlapping of the two beams is confirmed by optical microscopy after the depth profile experiments, as is shown in Figure 1.

The C_{60} primary ion source, obtained from Ionoptika Ltd. (Southhampton, UK), was directed to the target at an angle of 40° relative to the surface normal. Details of the design of this source have been published [26]. The nominal kinetic energy of the C_{60}^+ beam was chosen as

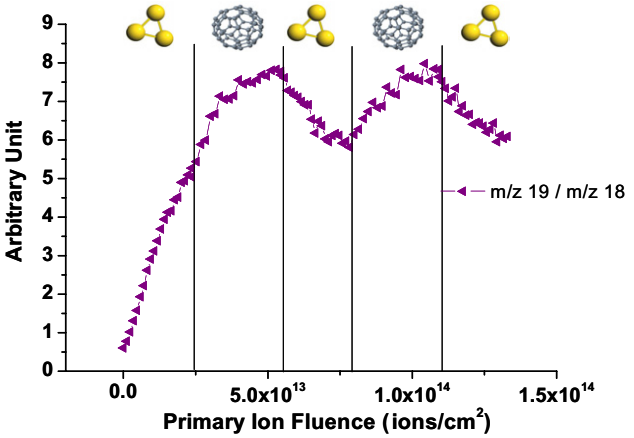

Figure 3. Plot of the ratio between *m/z* 19 to *m/z* 18 versus accumulated total ion dose.

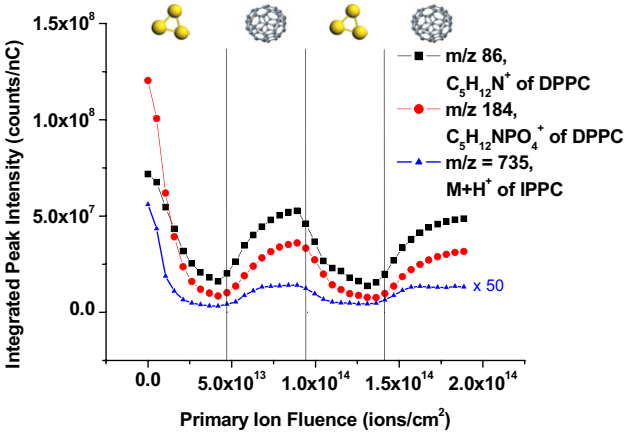

Figure 4. Depth profile plot of the DPPC molecular ion M + H^+ (*m/z* = 735) and principle DPPC headgroup fragments phosphocholine $C_5H_{15}NPO_4^+$ (*m/z* = 184) and choline $C_5H_{12}N^+$ (*m/z* = 86) secondary ion signal intensities versus the primary ion dose accumulated during alternative bombardment with Au_3^+ and C_{60}^+. The sputter projectile used over a specified primary ion dose is illustrated in the figure.

20 keV with a DC beam current of about 0.1 nA and a probe size of typically about 20 μm in diameter. Contribution of ions other than C_{60}^+, for example C_{60}^{++}, was minimized to less than 20% by keeping the electron impact ionization energy in the source below 40 eV. The Au cluster ion source was also obtained from Ionoptika Ltd, and was equipped with a Wien filter for selecting Au_3^+ projectiles. A kinetic energy of 20 keV was employed with dc beam currents of 0.16 nA. The probe size from this liquid metal ion source is about 200 nm.

XPS

The X-ray Photoelectron Spectrometry (XPS) image was obtained by a Kratos Analytical Axis Ultra instrument (Kratos, NY). Samples were analyzed using a monochromatic aluminum source (1486.6 eV) at a power of 280 W. The takeoff angle was set to be 90° with respect to sample plane. Images were recorded in the low-magnification mode (80 eV pass energy, step size 0.2 eV). Charge on the surface is neutralized by low-energy electrons.

Results and Discussions

This work is focused on developing an efficient and straightforward approach to compare different cluster projectiles employed in molecular depth profiling with time of flight secondary ion mass spectrometry. Two commonly used and representative cluster projectiles, C_{60}^+ and Au_3^+, are overlapped and switched during the depth profiling of two types of organic films. Mass spectra are collected using the C_{60}^+ source in the low-fluence mode.

Beam-Switching Depth Profiles of Peptide-Doped Film with Au_3^+ and C_{60}^+

The results of a depth profile of a film of trehalose doped with 1% GGYR alternately with Au_3^+ and C_{60}^+ overlapped on the same area, are shown in Figure 1. The depth profile starts with Au_3^+ bombardment, followed by a nearly equal dose of C_{60}^+ bombardment. In total, 3 cycles of Au_3^+ bombardment and 2 cycles of C_{60}^+ bombardment are performed on the film to confirm repeatability.

As shown, the molecular ions of both the peptide GGYR (*m/z* 452) and trehalose (*m/z* 325) exhibit similar trends. After the initial surface fluctuation observed for Au_3^+ bombardment, reported in previous studies [9], both molecular ion signals recover to different extents upon switching from Au_3^+ to C_{60}^+. After the signals reach a steady-state, an immediate decline in signal intensity is observed when the sputter source is switched to Au_3^+. Since all spectra are obtained with the same ion source, the fact that the molecular signals increase with C_{60}^+ bombardment and decrease with Au_3^+ bombardment suggests that sputtering with Au_3^+ creates more chemical damage to the sample surface than sputtering with C_{60}^+. To measure the degree of chemical damage, a plot has been made of the ratio between a fragment ion of GGYR at *m/z* 437 and the molecular ion at *m/z* 452 as a function of the ion dose accumulation and is illustrated in Figure 2a. As shown, the amount of molecular fragmentation increases with the increasing Au_3^+ fluence. Then, after switching to the C_{60}^+ source, the degree of fragmentation increases and reaches a steady-state before Au_3^+ is used again and the fragmentation goes up accordingly. These results agree qualitatively with previous studies where the damage cross sections of the two cluster ion sources were calculated from the ero-

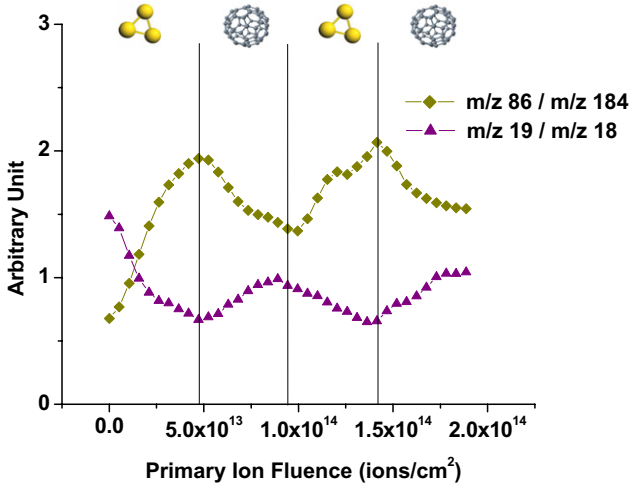

Figure 5. Plots of the ratio between the fragmented choline ion $C_5H_{12}N^+$ (*m/z* = 86) and the phosphocholine ion $C_5H_{15}NPO_4^+$ (*m/z* = 184) and the ratio between H_3O^+ (*m/z* = 19) and H_2O^+ (*m/z* = 18) (as a measure of surface protons accumulated during the depth profile) versus primary ion dose accumulated during alternative bombardment with Au_3^+ and C_{60}^+.

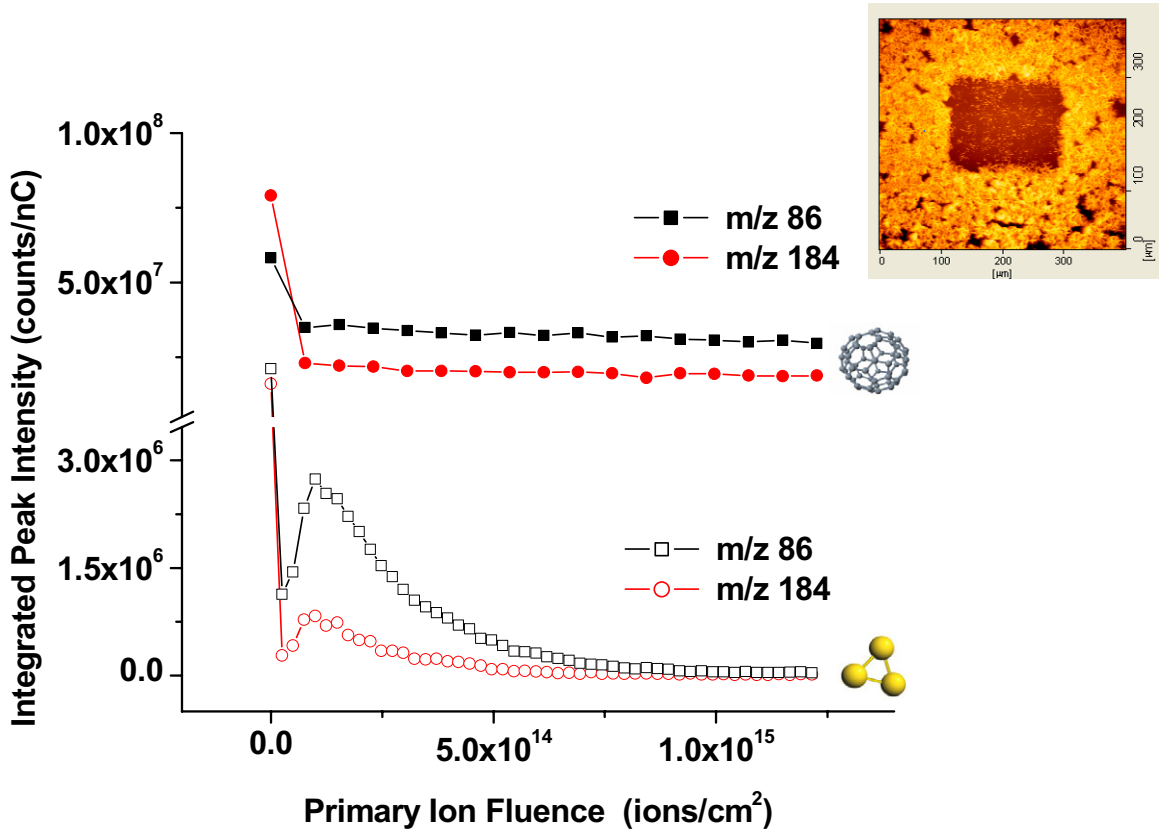

Figure 6. Depth profile plot of DPPC molecular fragments phosphocholine $C_5H_{15}NPO_4^+$ (m/z = 184) and choline $C_5H_{12}N^+$ (m/z = 86) secondary ion intensities versus primary ion dose. Solid symbols represent secondary ion intensities acquired during a depth profile using C_{60}^+ only (as both the sputter source and the analysis source) and open symbols represent secondary ion intensities acquired during a depth profile using Au_3^+ only. The inset is an AFM image of a dry, porous DPPC film bombarded with C_{60}^+ at 200 × 200 μm^2 field of view. Image is taken at a 400 × 400 μm^2 field of view and indicates the film is 1000 nm thick with a 100 nm surface roughness.

sion dynamics model as 5 nm^2 for C_{60}^+ and 14 nm^2 for Au_3^+ [9].

The signal of Au_3^+ (m/z 591) during the depth profile is also plotted in Figure 1 to illustrate the presence of gold atoms in the sample. The Au_3^+ ion intensity is used because there is more signal background interference at Au_1^+ (m/z 197). The trend shows an increasing presence of Au with Au_3^+ bombardment and a decrease of the Au_3^+ signal upon C_{60}^+ bombardment, which has, except for the first cycle, the exact opposite trend of the molecular ions of the peptide and the trehalose molecule. The fact that the Au_3^+ signal intensity at m/z 591 mirrors the Au_3^+ ion bombardment dose supports the previous observation that Au_3^+ bombardment causes implantation of gold into the sample surface. Not only have the Au cluster peaks been seen in the mass spectrum, [9] but the XPS Au 4f signal is also observed from inside of the crater as shown in Figure 2b. The Au is removed by subsequent C_{60}^+ sputtering, as shown in Figure 1. Hence, C_{60}^+ bombardment not only recovers the molecular signals by removing the damage under Au_3^+ sputtering, but it also removes the surface modification caused by Au_3^+ sputtering.

Another interesting characteristic to compare between the two ion sources is the ratio between m/z 19 and m/z 18, presumably H_3O^+ and H_2O^+. The SIMS spectra of organic molecules usually include varying amounts of these species presumably due to recombination of oxygen containing fragment ions produced during the bombardment. In recent work, [22, 24] this ratio has been used to help explain the high ion yields associated with cluster ion sources. The hypothesis is that cluster bombardment is more efficient at producing protons via a bond breaking mechanism in the compressed region directly underneath the penetrating cluster. These protons would remain in the surface region after bombardment and would be available for attachment to neutral molecules to form the quasimolecular ions during subsequent bombardment events. Since high mass molecules will be moving more slowly than lighter ions, it is expected that this effect should dominate in the higher mass region. This ratio will then be referred to as the proton factor and is plotted in Figure 3. As shown, the proton factor increases as Au_3^+ bombards the surface initially, which agrees well with observations from other work [24]. After switching to

C_{60}^+, this trend continues until Au_3^+ is switched back and the factor starts decreasing to about the same level as before C_{60}^+ bombardment. The result suggests that Au_3^+ and C_{60}^+ are both effective proton producers with C_{60}^+ being slightly more effective [24]. This observation could also be another reason that the molecular ion signals are more intense with C_{60}^+ bombardment than with Au_3^+ bombardment. Similar results are obtained from pure trehalose films or trehalose films doped with other peptides, such as VGSE.

Switch-Depth-Profiling DPPC Film with Au_3^+ and C_{60}^+

The response of a DPPC film on Si alternately bombarded by Au_3^+ and C_{60}^+ is shown in Figure 4. The molecular ion of DPPC at *m/z* 735 behaves in a qualitatively similar fashion to the principle head group fragment ions at *m/z* 184 and *m/z* 86 [27, 28]. Upon initial bombardment by Au_3^+, the *m/z* 735 peak intensity drops by more than an order of magnitude, presumably due to chemical damage accumulation. Upon bombardment with C_{60}^+, the peak intensity recovers to a degree due to the removal of some of this chemical damage. The fragment ions follow the same trend, although the magnitude of the initial decline of the signal intensity is not as pronounced as it is for the molecular ion.

The increased level of fragmentation with Au_3^+ versus C_{60}^+ is apparent in this film as shown in Figure 5. The ratio of peak intensities at *m/z* 86 to *m/z* 184 clearly increase under Au_3^+ bombardment, and decrease under C_{60}^+ bombardment. This result parallels the result reported for the peptide/trehalose films. Moreover, the ratio of *m/z* 19 to *m/z* 18 exhibits the same basic trend as reported for the peptide films as shown in Figure 5. Hence, the enhanced proton factor associated with C_{60}^+ bombardment is observed in the lipid films as well.

Finally, it is interesting to consider the issue of Au implantation during the depth profiling experiments. In contrast to the protein/sugar films, no Au signal could be observed in the mass spectrum even after an Au_3^+ fluence of 10^{15} ions/cm^2. The detailed depth profile over this fluence range is shown in Figure 6 for the principle fragment ions using both projectiles. There is an unusual increase in fragment ion intensity at an Au_3^+ fluence of $\sim 2 \times 10^{14}$ ions/cm^2. We speculate that this effect is a manifestation of Au implantation since this type of fluctuation is not observed during C_{60}^+ etching, and it parallels the behavior of the peptide/sugar film reported previously [9]. The reason why no Au^+ ion peaks are observed in the mass spectrum is not currently known, but could involve sampling depth or ionization efficiency issues.

Conclusions

This work provides a method that yields a direct and efficient comparison between sputtering of organic films by C_{60}^+ and Au_3^+ with the aim of optimizing cluster projectiles for molecular depth profiling experiments. The beam-switching depth profile results of a peptide-doped trehalose film and a spin-coated DPPC film support previous qualitative observations that there is more damage associated with Au_3^+ bombardment along with associated Au implantation. Moreover, C_{60}^+ bombardment is found to be able to remove the damage and the implanted Au effectively.

The implication of these results for 3D imaging experiments is interesting to ponder. For these films, it is possible to estimate the effective efficiency of molecular ion formation from the intensity of the peak in the mass spectrum, the measured erosion rate using AFM or quartz crystal microbalance measurements and the known fluence of the incident projectile. Very roughly, these numbers are still small, even with cluster bombardment. For the peptide molecular ion, for example, only about 3×10^{-6} molecular ions are detected for each neutral molecule equivalent of ejected peptide [9]. With respect to imaging experiments, a 100 nm $\times$ 100 nm pixel contains roughly 10^4 molecules, assuming 100% concentration. From these data, clearly more than one layer can be utilized to sum intensity into the pixel, but to retain the intrinsic depth resolution of molecular depth profiling, it would be prudent to restrict this summation to less than 10 nm, or about 10^5 molecules per voxel. Hence, the best possible intensity at this lateral resolution will only be 0.3 ions/pixel. To achieve adequate sensitivity for imaging with this sort of lateral resolution, it is obvious that the only way will be to increase the ionization efficiency.

Acknowledgments

The authors acknowledge Christopher Szakal for part of the sample preparations, the National Institutes of Health for providing funds to construct the C_{60} source, and National Science Foundation and Department of Energy for providing graduate student support.

References

1. Jones, E. A.; Lockyer, N. P.; Vickerman, J. C. Mass Spectral Analysis and Imaging of Tissue by TOF-SIMS—the Role of Buckminsterfullerence, C60+, Primary Ions. *Int. J. Mass Spectrom.* **2006,** in press.
2. Winograd, N. The Magic of Cluster SIMS. *Anal. Chem.* **2005,** *77,* 142A–149A.
3. Winograd, N.; Postawa, Z.; Cheng, J.; Szakal, C.; Kozole, J.; Garrison, B. J. Improvements in SIMS Continue. Is the End in Sight? *Appl. Surf. Sci.* **2006,** *252(19),* 6836-6843.
4. Cornett, D.; Lee, T.; Mahoney, J. Matrix-Free Desorption of Biomolecules Using Massive Cluster-Impact. *Rapid Commun. Mass Spectrom.* **1994,** *8,* 996–1000.
5. Tempez, A.; Schultz, J. A.; Della-Negra, S.; Depauw, J.; Jacquet, D.; Novikov, A.; Lebeyec, Y.; Pautrat, M.; Caroff, M.; Ugarov, M.; Bensaoula, H.; Gonin, M.; Fuhrer, K.; Woods, A. Orthogonal Time-of-Flight Secondary Ion Mass Spectrometric Analysis of Peptides Using Large Gold Clusters as Primary Ions. *Rapid Commun. Mass Spectrom.* **2004,** *18,* 371–376.
6. Gillen, G.; Roberson, S. Preliminary Evaluation of an SF5+ Polyatomic Primary Ion Beam for Analysis of Organic Thin Films by Secondary Ion Mass Spectrometry. *Rapid Commun. Mass Spectrom.* **1998,** *12,* 1303–1312.
7. Mahoney, C. M.; Roberson, S. V.; Gillen, G. Depth Profiling of 4-Acetamidophenol-Doped Poly(Lactic Acid) Films Using Cluster Secondary Ion Mass Spectrometry. *Anal. Chem.* **2004,** *76,* 3199–3207.
8. Cheng, J.; Winograd, N. Depth Profiling of Peptide Films with TOF-SIMS and a C-60 Probe. *Anal. Chem.* **2005,** *77,* 3651–3659.

9. Cheng, J.; Wucher, A.; Winograd, N. Molecular Depth Profiling with Cluster Ion Beams. *J. Phys. Chem. B* **2006,** *110,* 8329–8336.
10. Wagner, M. S. Molecular Depth Profiling of Multilayer Polymer Films Using Time-of-Flight Secondary Ion Mass Spectrometry. *Anal. Chem.* **2005,** *77,* 911–922.
11. Wagner, M. S.; Gillen, G. Impact Energy Dependence of SF5+ Ion Beam Damage of Poly(Methyl Methacrylate) Studied by Time-of-Flight Secondary Ion Mass Spectrometry. *Appl. Surf. Sci.* **2004**, *231/232,* 169–173.
12. Sostarecz, A. G.; McQuaw, C. M.; Wucher, A.; Winograd, N. Depth profiling of Langmuir-Blodgett films with a Buckminsterfullerene Probe. *Anal. Chem.* **2004,** *76,* 6651–6658.
13. Breitenstein, D.; Rommel, C.; Mollers, R.; Wegener, J.; Hagenhoff, B. **2006,** unpublished.
14. Touboul, D.; Halgand, F.; Brunelle, A.; Kersting, R.; Tallarek, E.; Hagenhoff, B.; Laprevote, O. Tissue Molecular Ion Imaging by Gold Cluster Ion Bombardment. *Anal. Chem.* **2004,** *76,* 1550–1559.
15. Touboul, D.; Kollmer, F.; Niehuis, E.; Brunelle, A.; Laprevote, O. Improvement of Biological Time-of-Flight-Secondary Ion Mass Spectrometry Imaging with a Bismuth Cluster Ion Source. *J. Am. Soc. Mass Spectrom.* **2005,** *16,* 1608–1618.
16. Davies, N.; Weibel, D. E.; Blenkinsopp, P.; Lockyer, N.; Hill, R.; Vickerman, J. C. Development and Experimental Application of a Gold Liquid Metal Ion Source. *Appl. Surf. Sci.* **2003,** *203,* 223–227.
17. Appelhans, A. D.; Delmore, J. E. Comparison of Polyatomic and Atomic Primary Beams for Ssecondary Ion Mass Spectrometry of Organics. *Anal. Chem.* **1989,** *61,* 1087–1093.
18. VanStipdonk, M. J.; Harris, R. D.; Schweikert, E. A. A Comparison of Desorption Yields from C-60(+) to Atomic and Polyatomic Projectiles at keV Energies. *Rapid Commun. Mass Spectrom.* **1996,** *10,* 1987–1991.
19. Pacholski, M. L.; Winograd, N. Imaging with Mass Spectrometry. *Chem. Rev.* **1999,** *99,* 2977–3005.
20. Fletcher, J. S.; Conlan, X. A.; Jones, E. A.; Biddulph, G.; Lockyer, N. P.; Vickerman, J. C. TOF-SIMS Analysis Using C-60-Effect of Impact Energy on Yield and Damage. *Anal. Chem.* **2006,** *78,* 1827–1831.
21. McMahon, J. M.; Dookeran, N. N.; Todd, P. J. Organic Ion Imaging Beyond the Limit of Static Secondary Ion Mass Spectrometry. *J. Am. Soc. Mass Spectrom.* **1995,** *6,* 1047–1058.
22. Wucher, A.; Sun, S.; Szakal, C.; Winograd, N. Molecular Depth Profiling of Histamine in Ice Using a Buckminsterfullerene Probe. *Anal. Chem.* **2004,** *76,* 7234–7242.
23. Kozole, J.; Szakal, C.; Kurczy, M.; Winograd, N. *Appl. Surf. Sci.* **2006,** *252(19),* 6789-6792.
24. Conlan, X. A.; Lockyer, N. P.; Vickerman, J. C. Is Proton Cationization Promoted by Polyatomic Primary Ion Bombardment During Time-of-Flight Secondary Ion Mass Spectrometry Analysis of Frozen Aqueous Solutions? *Rapid Commun. Mass Spectrom.* **2006,** *20,* 1327–1334.
25. Braun, R. M.; Blenkinsopp, P.; Mullock, S. J.; Corlett, C.; Willey, K. F.; Vickerman, J. C.; Winograd, N. Performance Characteristics of a Chemical Imaging Time-of-Flight Mass Spectrometer. *Rapid Commun. Mass Spectrom.* **1998,** *12,* 1246–1252.
26. Weibel, D.; Wong, S.; Lockyer, N.; Blenkinsopp, P.; Hill, R.; Vickerman, J. C. A C-60 Primary Ion Beam System for Time of Flight Secondary Ion Mass Spectrometry: Its Development and Secondary Ion Yield Characteristics. *Anal. Chem.* **2003,** *75,* 1754–1764.
27. Roddy, T. P.; Cannon, D. M., Jr.; Ostrowski, S. G.; Ewing, A. G.; Winograd, N. Proton Transfer in Time-of-Flight Secondary Ion Mass Spectrometry Studies of Frozen-Hydrated Dipalmitoylphosphatidylcholine. *Anal. Chem.* **2003,** *75,* 4087–4094.
28. McMahon, J. M.; Short, R. T.; McCandlish, C. A.; Brenna, J. T.; Todd, P. J. Identification and Mapping of Phosphocholine in Animal Tissue by Static Secondary Ion Mass Spectrometry and Tandem Mass Spectrometry. *Rapid Commun. Mass Spectrom.* **1996,** *10,* 335–340.